Available online at www.sciencedirect.com
ScienceDirect
Cold Regions Science and Technology 46 (2006) 167–180
cold regions science and technology
www.elsevier.com/locate/coldregions

Capacitance probe measurements of brine volume and bulk salinity in first-year sea ice

Lars G.E. Backstrom *, Hajo Eicken

Geophysical Institute, University of Alaska Fairbanks, PO Box 757320, Fairbanks, AK 99775-7320, USA

Received 28 May 2006; accepted 16 August 2006

Abstract

First-year sea ice plays an important role in the global climate system. It changes the physical properties of the surface of the polar oceans, and modifies the energy and mass transfer between the ocean and the atmosphere. An understanding of the way sea ice affects ocean–atmosphere exchange requires detailed knowledge of the evolution of ice physical properties, which are governed by its temperature and bulk salinity. To this effect, we assessed the utility of commercially available capacitance probes in determining the salinity evolution of first-year sea ice. Measurements of the complex dielectric permittivity, $\varepsilon = \varepsilon' - i\varepsilon''$, at 50 MHz were carried out in land-fast ice in McMurdo Sound, Antarctica, and in the Chukchi Sea near Barrow, Alaska. For comparison, we also deployed the probes in artificial, young sea ice in an outdoor tank experiment in Fairbanks, AK. The dielectric permittivity data compare well with predictions from a dielectric mixture model.

We have derived a simple relation that allows for the derivation of brine volume fraction and bulk salinity in columnar first-year sea ice from the real part of the complex dielectric permittivity. For ice at temperatures below the percolation threshold, the error in the derived bulk salinity is less than 15%. The dependence of dielectric permittivity on brine inclusion morphology needs to be taken into consideration, and measurements indicate that changes in pore morphology are recorded in the capacitance measurements.

In this paper we use the real part, ε', of the complex dielectric permittivity to study the bulk salinity of bubble-free columnar ice. Further investigations, using the imaginary part of the complex dielectric permittivity, ε'', will make it possible to use the same probes to measure the bulk salinity and pore morphology of other types of ice, e.g., frazil, platelet, and multi-year ice.

Keywords: Capacitance; Bulk salinity; Complex dielectric permittivity; Brine volume fraction; Brine inclusion morphology; Sea ice

1. Introduction

At its maximum extent during Antarctic winter, sea ice covers approximately 7% of the Earth's surface, with first-year sea ice making up over 80% of the ice in the southern polar ocean, and about 45% of the ice in the Arctic Ocean (Comiso, 2003). It is only a thin layer, measured in meters, compared to the thousands of meters of unfrozen ocean beneath, but it profoundly changes the physical characteristics of the ocean surface. Sea ice increases the albedo of the ocean, decreases the amount of moisture, the amount of heat, and the momentum transferred between the ocean and the atmosphere. Sea ice, therefore, plays an important part in the global climate system (Maykut, 1986; Bitz and Lipscomb, 1999). Since the ice cover is typically

* Corresponding author. Tel.: +1 907 474 7818; fax: +1 907 474 7290.
E-mail address: larsg@gi.alaska.edu (L.G.E. Backstrom).

0165-232X/$ - see front matter © 2006 Elsevier B.V. All rights reserved.
doi:10.1016/j.coldregions.2006.08.018

relatively thin, it is also very sensitive to perturbations in the atmosphere–ocean heat flux (Dieckmann and Hellmer, 2003).

The physical properties – thermal, mechanical, and electromagnetic – of sea ice are governed by its temperature and salinity, which control the volume fraction of brine within the ice matrix, as well as the morphology of brine inclusions (Weeks and Ackley, 1986; Eicken, 2003). Due to the inaccessibility of the ice cover, it is comparatively difficult to measure these properties in situ within naturally growing sea ice. The salinity in particular has hitherto been difficult to measure in the field. The easiest and most widespread method is to measure the bulk salinity from core samples. One drawback of this method, however, is brine drainage from porous ice (Cox and Weeks, 1986), and, as noted above, access to the study area can be difficult. Therefore, by necessity, the temporal and spatial resolution of this method is variable and tends to be poor.

Schwarzacher (1959) and Untersteiner (1968) studied the salinity distribution and desalination processes in multi-year ice. Based on their own experiments and work by Nakawo and Sinha (1981), Cox and Weeks (1975, 1988) developed a numerical model of the salinity profile of first-year sea ice that is valid before the flushing of the ice during summer melt. However, their model fails to capture the high-frequency variations in the salinity profile due to rapid changes in meteorological conditions (Cox and Weeks, 1988). Furthermore, it tends to underestimate the salinity of thin ice and overestimate the salinity of thick ice (Cox and Weeks, 1988), and it does not describe the large horizontal variations observed in the field (Bennington, 1967; Tucker et al., 1984).

In this paper, we present a non-destructive method suitable for obtaining long time series of bulk salinity and relative brine volume at centimeter resolution in naturally growing sea ice. This work builds on studies by Vant (1976), Vant et al. (1978), and Morey et al. (1984), who conducted thorough theoretical and experimental investigations of the dielectric properties of sea ice. Vant (1976) also provides an exhaustive overview of previous work. Arcone et al. (1986) showed that the complex dielectric properties of natural sea ice change with time, opening the possibility to track changes in bulk salinity and ice microstructure. A non-destructive method to track changes in ice salinity was recently presented by Notz et al. (2005), based on changes in impedance between platinum wires frozen into the ice. Here, we employ a commercially available capacitance probe to derive complex dielectric permittivity data of the bulk sea ice at 50 MHz. The dependence of the real part of the complex dielectric permittivity on brine volume fraction and brine salinity is then utilized to derive the bulk salinity of the ice, in conjunction with in situ temperature measurements.

2. Methodology

2.1. Complex dielectric permittivity of sea ice

Naturally occurring sea ice is a complex dielectric mixture whose three main components are pure ice, liquid brine, and air bubbles. At temperatures below −22.9 °C, precipitated salts also become a significant component, and under certain conditions particle inclusions and microorganisms can form part of the mixture.

Each of the components of sea ice, or similar mixtures, has its own distinctive dielectric properties. Their relative concentrations and distribution determine the dielectric properties of the sea ice, or mixture (Stogryn, 1987; Chelidze and Gueguen, 1999; Chelidze et al., 1999; Fabbri et al., 2006). For this study we do not consider surface effects of polarization or clustering of components (Chelidze and Gueguen, 1999; Chelidze et al., 1999; Moore and Maeno, 1993). Clustering, or the development of discrete continuous paths of the conductive component, occurs near the percolation threshold only; and we as yet lack information about the ice-brine interface in the brine inclusions.

In this paper we will limit our study to the complex dielectric permittivity of columnar first-year sea ice, which makes up most of the interior of the ice, below or near the percolation threshold, 50–70‰ (Weeks and Ackley, 1986; Golden et al., 1998). The percolation threshold occurs when the relative brine volume becomes so large that the discrete brine inclusions start to connect and form networks, enabling gravitational drainage. If the salinity of the ice is 5‰, which is a valid assumption for the interior of Arctic first-year ice, the percolation threshold is reached around a temperature of −5 °C (Golden et al., 1998) Thus, we can assume that we have a mixture of pure ice and brine only, with the brine occurring in discrete pockets within the ice matrix. We leave to future studies frazil and platelet ice with their irregular crystal structure and brine inclusion morphology, as well as ice close to its melting point and multi-year ice with their complex mixtures, including air bubbles.

The complex dielectric permittivity, $\varepsilon = \varepsilon' - i\varepsilon''$, of both of these materials is described by the Debye (1929) equation:

$$\varepsilon = \varepsilon_\infty + \frac{\varepsilon_l - \varepsilon_\infty}{1 + i\omega\tau} - \frac{i\sigma}{\varepsilon_0\omega} \quad (1)$$

where ε is the complex frequency-dependent dielectric permittivity; ε_l is the static complex dielectric permittivity of the material; ε_∞ is the high-frequency complex dielectric permittivity of the material; ε_0 is the complex dielectric permittivity of free space; ω is the angular frequency of the signal; τ is the relaxation time of the material; σ is the ionic conductivity of the material; i is $(-1)1/2$.

The studies by Morey et al. (1984) and Arcone et al. (1986) showed that ε' depends mostly on the relative brine volume V_b/V, and less on the brine inclusion geometry. For the imaginary part of the complex dielectric permittivity, ε'', the relation is the opposite (Morey et al., 1984). However, Kovacs and Morey (1979), and Morey et al. (1984) showed that crystal orientation does affect ε', with a reduction for a configuration with the electrical field vector parallel to the c-axis of the ice crystals, as discussed in more detail below.

2.2. Instrumentation

We chose to use the Stevens Water Monitoring Systems Hydraprobe for this study. It was originally developed by Campbell (1988, 1990) for non-destructive, in situ measurements of soil moisture. The rugged design and lack of need for maintenance makes it ideal for semi-permanent emplacement, and for long-term measurements in frozen materials (Romanovsky and Yoshikawa, personal communication, 2000; Yoshikawa et al., 2004).

The Hydraprobe is a coaxial probe with a central tine surrounded by three equally spaced outer tines, all made out of stainless steel. The three outer tines are held at ground potential, and a voltage is applied to the central tine at 50 MHz frequency, resulting in a circularly polarized wave (see Table 1 for a list of relevant probe parameters; Campbell, 1990; Stevens Water Monitoring Systems, 1994). The probe head also contains a thermistor for temperature measurements. Since the thermistor is located inside the probe, it measures, strictly speaking, the temperature of the probe, but the probe has for the most part the same temperature as the surrounding ice. The error for the temperature given in Table 1 is for the entire temperature range; the probe is designed to operate at. Comparison with arrays of thermistors, deployed in conjunction with the Hydraprobe arrays (see below), indicate an uncertainty in the temperature of ~0.2 °C over the temperature intervals studied here.

Table 1
Technical specifications of the Hydraprobe capacitance probe

Tine length (mm)	57
Tine diameter (mm)	4
Probe radius (mm)	15
Sensing volume (mm^3)	13,000
Dielectric measurement error	±0.2
Specified temperature measurement error (K)[a]	±0.6

[a] The error in temperature ±0.6 K is for the entire operating range of −15–65 °C. For the temperature range in our experiments the error was considerably smaller.

Brine volumes larger than 300‰ (Stevens Water Monitoring Systems, 1994), and large vertical variations in brine volume over a few centimeters in the skeletal layer of the bottom-most few centimeters of the ice, for instance, result in large errors that preclude further data analysis.

The output data are in the form of four voltages: V1–4, where V1–V3 give the capacitive and conductive response of the material, and V4 gives the temperature. The raw voltages were converted using a program supplied by Stevens Water Monitoring Systems.

In the field, the probes were connected to a Campbell CR10X datalogger. The measurements were made using a single-ended measurement without excitation over a ±2.5 V interval. The signal was integrated over 2.72 mS. The measurements were stored in Campbell Scientific SM716 storage modules, which were regularly changed, and data downloaded to PC laptops. The setup was powered by a 12-V marine battery, with the connection only switched on during measurements.

In the field we mounted the Hydraprobes on 2-in.-diameter PVC half pipes, which were deployed by drilling through thin, growing ice, with the tines protruding from the convex side. The ice was then allowed to embed the probes naturally. Examination of ice thin sections cut around probes revealed no major deviations from ice microstructure of standard congelation ice, i.e., a columnar ice crystal structure with subparallel, vertically oriented layers of brine between submillimeter ice lamellae. Visual inspection also indicates that ice crystals do not nucleate on the tines ahead of the advancing lower boundary of the ice (Cotter and Miner, personal communication, 2005; Notz et al., 2005).

The datalogger and storage module were deployed in insulated boxes on the ice, together with the batteries to keep them protected from the harsh environment and direct sunlight, and were recording data every 10–30 min.

Together with the arrays of capacitance probes in McMurdo and Barrow, two arrays of thermistors were deployed to measure the temperature profile of the ice. One array on each site was operated by the authors and the other was operated by colleagues from Victoria University, New Zealand. Their vertical spacing was

0.1 m (further details can be found in Pringle et al., submitted for publication).

At the time of deployment, at the time of probe extraction, and in between, 0.1-m-diameter ice cores were obtained through the entire thickness of the ice for stratigraphic analysis. The temperature of the cores was measured, and 0.1-m sections of the cores were melted for determination of salinity by using a YSI 30 conductivity probe (measurement error < 0.02 or < 1% of the bulk salinity, whichever is larger).

In both McMurdo and Barrow the experiment sites were chosen on undeformed land-fast ice, without leads or ridges nearby.

2.3. Laboratory and field experiments

2.3.1. Measurements in landfast sea ice in McMurdo Sound, Antarctica, July 10–November 11, 2002

An array of four Hydraprobes was deployed at 77.73°S 166.44°E on July 10, 2002 in the first-year landfast ice of McMurdo Sound, northwest of the Erebus ice tongue. The probes were deployed at depths of 0.85 m, 1.05 m, 1.25 m, and 1.45 m. One thermistor array was deployed 3.4 m away, and the other 100 m away. The site was tended to by members of the overwintering crew at the New Zealand Scott Base. Ice thickness at deployment was approximately 1.2 m. The arrays were retrieved on November 11 by the authors and colleagues from Victoria University, New Zealand. A core drilled at the site at this time indicated an ice thickness of 2.3 m.

Readings were taken every 30 min. For this analysis, we only consider data from the bottom-most two of the four probes. The two topmost probes were deployed within the drill hole, as the ice thickness was greater at deployment than anticipated, and the ice within the borehole is not considered representative of natural conditions at the site. The bottom-most probes were encased by the growing ice.

Air temperatures were obtained from Automatic Weather Station Pegasus North (77.958°S 166.5°E), operated by the Space Science and Engineering Center, University of Wisconsin–Madison, USA.

2.3.2. Measurements in landfast sea ice off Barrow, Alaska, February 2–June 4, 2003

An array of three Hydraprobes was deployed in the Chukchi Sea landfast ice, 156.67°W, 71.34°N, on February 2, 2003 in ice of 0.7 m thickness. The probes were deployed at depths of 0.4 m, 0.6 m, and 0.8 m below the upper surface of the ice. As in the McMurdo experiment, the thickness of the ice was underestimated, and only data from the lowermost probe are analyzed in this paper. The array was recovered on June 7 from ice with a thickness of 1.29 m. One thermistor array was deployed 1 m away from the dielectric probe array, and the other 50 m away.

Three cores were taken during the course of the experiment: one during deployment on February 2, one on April 8, 50 m away from the site but in ice of comparable thickness and microstructure, and one on June 4 when recovering the array.

Air temperature data have been obtained with a shielded thermometer mounted at 2 m height at the same site (data provided by D.K. Perovich, Cold Regions Research and Engineering Laboratory, Hanover, NH).

2.3.3. Outdoor ice tank experiment, Fairbanks, AK, February 8–April 20, 2003

To compare the field results with an experiment under controlled conditions, probes were deployed in a 1.5-m^3 outdoor tank at the Geophysical Institute of the University of Alaska Fairbanks. The tank was filled with spring water and Instant Ocean artificial sea salt from Aquarium Systems to simulate seawater with salinity of 32‰.

The tank was fitted with both a thermostat and heater to regulate ice growth. A pressure relief valve system connected to a glycol reservoir prevented pressure build-up in the tank, which could potentially push brine upwards through the ice. A low-speed circulation pump to mix the water was also fitted to the tank, but it malfunctioned at an unknown time during the experiment. Ice thickness was measured twice daily with a weighted wire gauge frozen into the ice. On April 15, when the last core was obtained, the ice thickness exceeded 0.45 m.

Four Hydraprobes were fitted in a plastic mesh: two at 0.03 m, and two at 0.19 m depth in the water. We have used data from only one of the lowermost probes for this analysis due to the large variations in temperature and the later radiative heating of the ice that complicated analysis of these data from the topmost probes and due to malfunction of the other probe at 0.19 m depth in the ice.

Air temperature data, as provided by the National Weather Service, comes from the meteorological station at Fairbanks International Airport, situated 5 km from the experiment site.

3. Results and analysis

3.1. Field data

3.1.1. McMurdo Sound

The output from the Hydraprobes, together with air temperature data, is shown in Fig. 1. Because of the

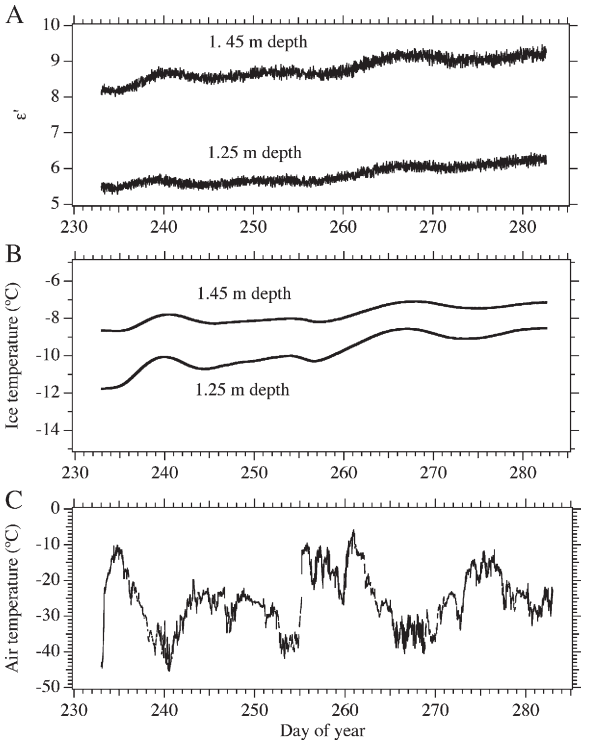

Fig. 1. Output from the Hydraprobe array deployed in the landfast ice in McMurdo Sound, Antarctica, 2002, between August 21 and October 9. The development with time for the two probes for ε' is shown in (A), the ice temperature in (B), and the air temperature in (C).

extreme conditions in McMurdo Sound, some data were lost due to equipment malfunctions. Here, we only consider data between August 21 and October 9.

Both the time series of the temperature and of ε′ are comparatively stable. This is due to the fact that the probes were deployed at a depth to which very little short-wave radiation penetrated, reducing the effect of the daily surface temperature variation. We see slight increases in the values of both the real part of the complex dielectric permittivity and ice temperature around August 28 (day 240) and September 25 (day 268), in response to atmospheric warming in the preceding days.

The salinity profile from the retrieved core is shown in Fig. 2. Comparison with other cores taken at the same time in the McMurdo Sound area and other data from the Antarctic (Eicken, 1992) indicates that the salinity profile is representative of Antarctic undeformed first-year ice. At a depth of 1.47 m in the core, approximately the depth of the lowermost probe, a layer of milky, less-transparent ice was observed, something occasionally associated with columnar ice growth in McMurdo Sound (Gow et al., 1998).

3.1.2. Barrow

The entire time series of the real part of the complex dielectric permittivity, ice, and air temperature data, from the time at which the probe was frozen into the ice cover on February 27 up to the retrieval of the array on June 7, is shown in Fig. 3. We have truncated the time series at ε′=20, so as to better be able to distinguish features in the data after freeze-in of the probe. On June 2 (day 153), there is a sharp increase in ε′, followed by a decrease. This coincides with the time when the ice is close to melting temperature throughout its thickness, around the period when we would expect substantial brine motion or even flushing, and corresponding changes in ice salinity.

The salinity data from the three cores retrieved during the experiment are shown in Fig. 4. The winter cores exhibit a typical C-shaped profile with high surface salinities and mostly stable salinities in the interior ice. After onset of surface melt, the surface 0.2 m of the ice desalinated rapidly due to meltwater flushing. A vertical thin section was produced from a core retrieved on February 24, 2003, 50 m distant, but from the same depth and type of ice as that embedding the probe. The ice consisted of large columnar crystals with horizontal *c*-axis alignment. Brine inclusions consisted of vertically oriented parallel layers and tubes of brine.

3.1.3. Ice tank experiment

The air temperature, ice temperature, and the real part of the complex dielectric permittivity as measured during the ice tank experiments are shown in Fig. 5. Due to technical difficulties, two periods of data were lost: February 21 to March 2 and March 18 to 23.

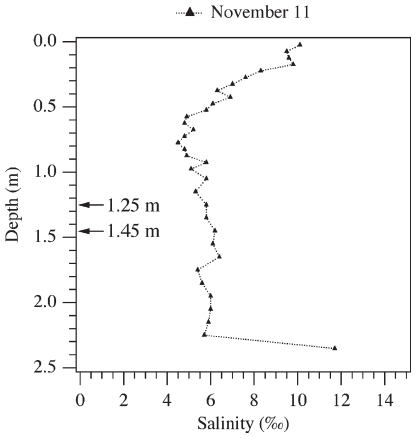

Fig. 2. Salinity profile from the core retrieved November 11, 2002, 1.2 m away from the Hydraprobe array in McMurdo Sound. The arrows indicate the approximate depths of the probes.

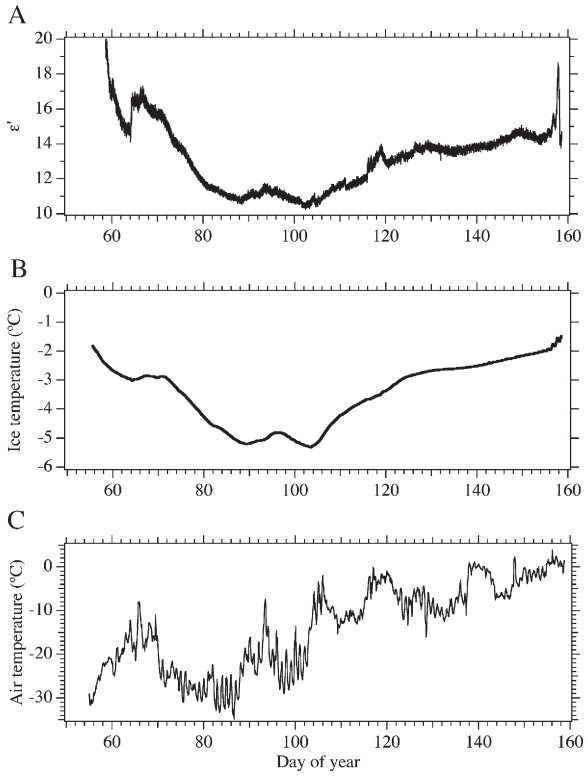

Fig. 3. Output from the Hydraprobe deployed at 0.8 m depth in the landfast ice at Barrow, Alaska, 2003, between February 27 and June 7. The development with time for the probe for ε' is shown in (A), the temperature recorded by the probe in (B), and the air temperature (C).

The probe was emplaced only 0.19 m below the upper surface of the ice, so the daily air temperature variations had an effect on both the ice temperature and on the complex dielectric permittivity, as measured by

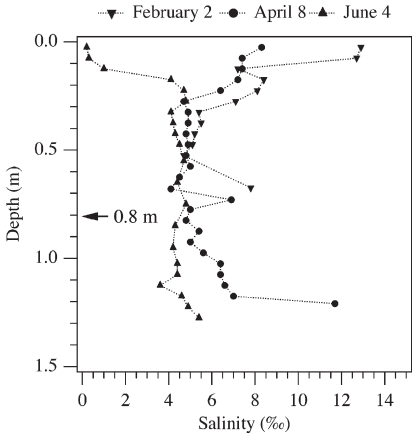

Fig. 4. Salinity profiles from the cores retrieved at or near the measurement site off Barrow, 2003, where the Hydraprobe array was deployed. The arrow indicates the approximate depth of the probe.

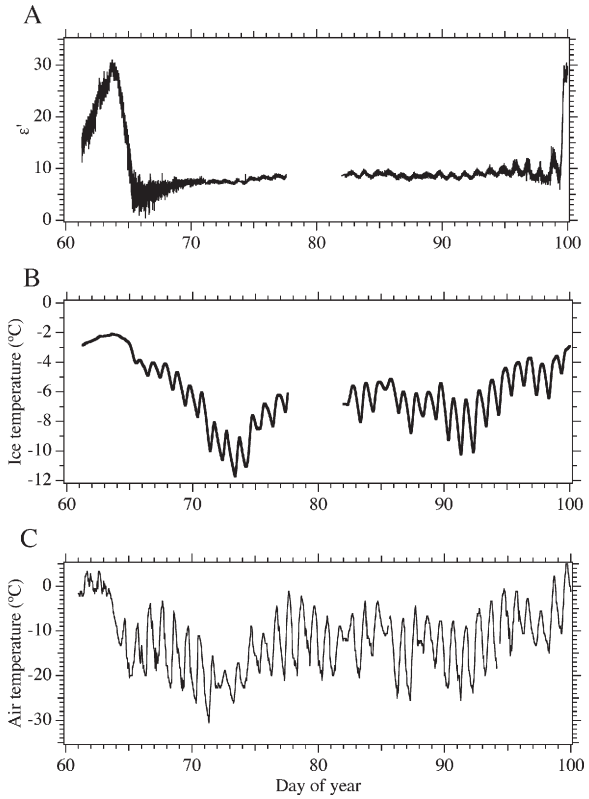

Fig. 5. Output from the Hydraprobe deployed in the ice tank experiment in Fairbanks, AK, 2003. The development with time for the probe for ε' is shown in (A), the ice temperature in (B), and the air temperature in (C). We show only data between March 2 and April 9 because of lost data at the beginning of the experiment, and flushing at the end of the experiment. Note the large daily variations in both temperature and ε' due to the variations in air temperature.

the probe. During the course of the experiment, diurnal temperature cycles and radiative heating of the probe (and the ice) became increasingly prominent.

Salinity data from the four cores retrieved during the course of the experiment are shown in Fig. 6. The ice cover was kept free of snow during the entire experiment. From the beginning of April onwards, the upper surface of the ice started to ablate. Later, with increasing temperatures, between April 5 and April 9 (days 94 and 99) a layer of meltwater formed on the upper surface of the ice. Even though the temperatures at a depth of 0.19 m were still comparatively low, the values of ε′ started to increase on April 9 (day 99), perhaps because of solar heating and local warming around the tines.

The cores here show rapid desalination, which can be expected with the large temperature gradients in the thin ice, and evidence of flushing in the upper 0.2 m of the core of April 15.

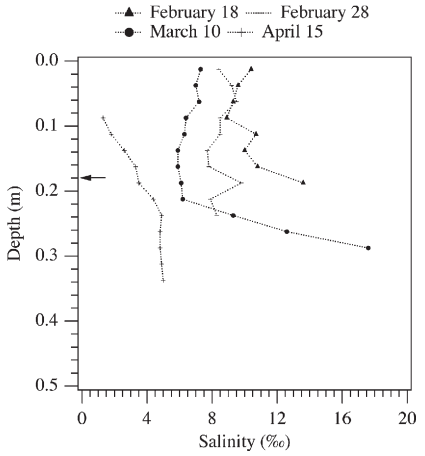

Fig. 6. Salinity profiles of the cores in the ice tank experiment. The arrow indicates the depth of the probe. The core retrieved on April 15 did not reach the bottom of the ice.

3.2. Deriving the bulk salinity of the ice from complex dielectric permittivity measurements

3.2.1. Apparent aspect ratio of brine inclusions in sea ice

The purpose of this study is to develop a method for determining the bulk salinity by measuring the complex dielectric permittivity and temperature of the ice. The complex dielectric permittivity of sea ice is not directly dependent on the bulk salinity, but rather on the relative brine volume of the ice, and the geometry of the brine inclusions.

In columnar ice, the brine inclusions take the form of ellipsoids below and around the percolation threshold, with the major axis vertical, or close to vertical (Assur, 1960; Cole and Shapiro, 1998; Eicken et al., 2000; Light et al., 2003). Addison (1970) showed that ε' has a dependency on the aspect ratio between the major and minor axes of the ellipsoidal brine inclusions, with brine inclusions with large aspect ratios contributing relatively more to the total ε' than brine inclusions with smaller aspect ratios. Vant (1976), Golden and Ackley (1980), Morey et al. (1984), and Arcone et al. (1986) adapt the dielectric mixture model developed by Tinga et al. (1973) to model the complex dielectric behavior of sea ice. Tinga's model assumes vertically aligned, ellipsoidal brine inclusions enclosed in a medium with complex dielectric permittivity ε_{MIX}, which is the complex dielectric permittivity of sea ice in this case.

This model is highly simplified, since in reality the dimensions of the brine inclusions vary from submillimeters to several millimeters in the vertical, and the inclusions are not symmetrical in the horizontal plane (Perovich and Gow, 1996; Eicken et al., 2000; Light et al., 2003). Arcone et al. (1986) stressed the need for a complex dielectric permittivity mixture model based on actual dimensions of the brine inclusions, and not only their aspect ratios.

Cole and Shapiro (1998) estimated an average aspect ratio of the brine inclusions in Arctic ice of ~9 in their sample from the ice interior. Their sample was taken from a depth of 0.8 m in the landfast ice in the Chukchi Sea outside Barrow, Alaska. Light et al. (2003) showed that around 50% of all brine inclusions in their three samples from the columnar interior of Arctic sea ice had aspect ratios between 10 and 20, and that these values changed little between −15 and −5 °C, but increased as the ice approaches melting temperature.

Tinga's model requires an average value of the aspect ratios of the brine inclusions. Still, using Tinga's relation will allow a first assessment of linkages between our permittivity measurements and in situ salinities. To be able to use Tinga's relation we must first, however, cast it in terms of the brine volume and bulk salinity of the ice:

$$\frac{\varepsilon_{AV}-\varepsilon_1}{\varepsilon_1} = \frac{V_2}{V_1} * \frac{\varepsilon_2-\varepsilon_1}{[-(V_2/V_1)n^*(\varepsilon_2-\varepsilon_1)+n(\varepsilon_2-\varepsilon_1)+\varepsilon_1]} \quad (2)$$

where V_2 is the brine volume; $V_1$is the pure ice volume; n is the depolarization coefficient which is dependent on the eccentricity of the ellipsoids; ε_1 is the complex dielectric permittivity of pure ice; ε_2 is the complex dielectric permittivity of brine; and ε_{AV} is the complex dielectric permittivity of the sea ice mixture.

The full method of calculating the temperature-dependent complex dielectric permittivity of pure ice and brine, ε_1 and ε_2, is given in Vant (1976).

The dimensions of the brine inclusions cannot be considered small in comparison to the probe dimensions (Stevens Water Monitoring Systems, 1994; Campbell, 1988; Cole and Shapiro, 1998; Eicken et al., 2000; Light et al., 2003); therefore, the ice will be assumed as anisotropic relative to the probe. The resulting value of ε_{MIX} measured by the probe is given by (Vant, 1976):

$$\varepsilon'_{MIX} = \frac{\varepsilon'_{AV(a)}}{2} + \frac{\varepsilon'_{AV(b)}}{2} \quad (3)$$

where $\varepsilon'_{AV(a)}$ is the real part of the complex dielectric permittivity with the electrical field parallel to the major axis of the brine inclusion; $\varepsilon'_{AV(b)}$ is the real part of the complex dielectric permittivity with the electrical field parallel to the minor axis of the brine inclusion.

The results of these calculations can be seen in Fig. 7. We have plotted ε' (dots) from the three experiments

against the corresponding temperatures. Bounding the experimental values are theoretical values calculated using Eqs. (2) and (3) (dashed lines with theoretical values in parenthesis). It is clear that for all the experiments, the apparent aspect ratio experienced by the probes correlates well with the aspect ratios measured by Cole and Shapiro (1998) and by Light et al. (2003). The aspect ratios measured by Eicken et al. (2000) are somewhat smaller. Furthermore, both the Barrow (B) and ice tank experiment (C) data sets show strong increases in the apparent aspect ratio with the ice temperature close to the melting or freezing of the ice, which is also in agreement with the observations by Light et al. (2003). Above the percolation threshold more and more networks of linked brine inclusions are formed, and the morphology of the brine inclusions becomes more complex than is covered by our model.

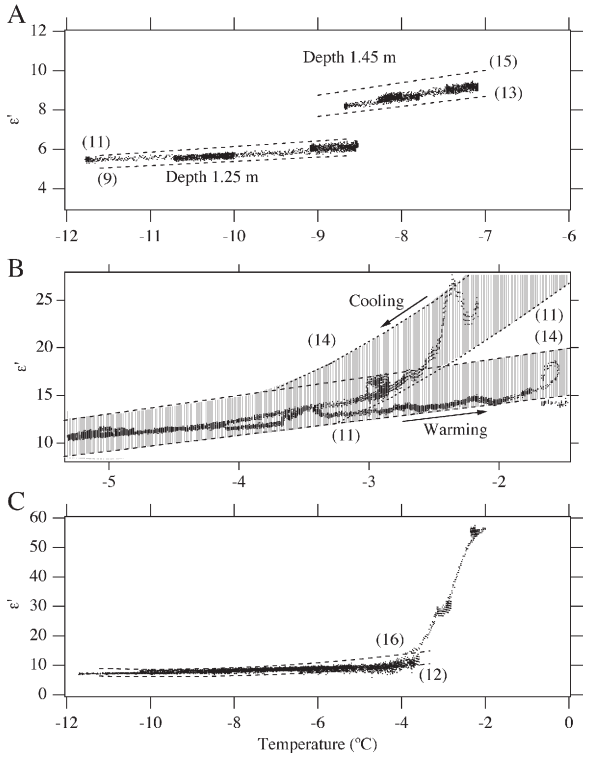

Fig. 7. The measured values of ε' (dots) compared with the theoretical aspect ratios (numbers within parentheses) of the brine inclusions calculated using Eq. (2): McMurdo Sound 2002 (A); Barrow 2003 (B); Fairbanks ice tank experiment 2003 (C). The values in parentheses correspond to aspect ratios of brine inclusions deemed realistic based on measurements in comparable types of ice. The dashed lines are the predictions of the model for these values. Since the values for Barrow, B, include both a cooling cycle and a warming cycle, the bounds are represented by a shaded area instead.

3.2.2. Establishing the relation between the real part of the complex dielectric permittivity and the bulk salinity of sea ice

As stated above, ε' is mainly dependent on the relative brine volume of the ice, V_b/V. Cox and Weeks (1983) and Leppäranta and Manninen (1988) developed a set of equations describing V_b/V as a function of the bulk salinity and temperature of the ice based on the phase relations in thermodynamic equilibrium:

$$\frac{V_b}{V} = \frac{\rho S}{F_1(T) - \rho S F_2(T)} \tag{4}$$

where ρ is $0.917 - 1.403 \times 10^{-4}\ T$ (the temperature dependent density of pure ice (Pounder, 1965); S is the bulk salinity of the ice; T is the temperature in °C; and $F_{1,2}(T)$ are empirical polynomial functions of temperature based on phase relations in the ice.

With ice temperature measured by the probes and the brine volume fraction estimated from the complex dielectric permittivity measurements, we can estimate the bulk salinity of the ice.

Fig. 8 shows the relative brine volume V_b/V as a function of ε' for all four probes. In the graph we have excluded data points where the temperature was higher than −2 °C, since interpretation of these data is complicated by probes extending into the skeletal layer, or into rotten ice, as well as potential solar heating. The chemical composition of the brine inclusions close to the melting point of ice is also uncertain. For reasons of clarity, we have chosen to plot only every 20th data point, even though we have used the entire data set for our calculations. For the Barrow measurements, we have also chosen to plot the periods from February 24 (day 55) to April 8 (day 98), and April 8 to June 7 (day 158) separately. We labeled these periods 'cooling' and 'warming'. The relative brine volumes have been calculated using Eq. (4) with the measured salinity data from the cores, assuming constant desalination rates between measurements. This is a valid assumption, supported by the research by Nakawo and Sinha (1981) and Cox and Weeks (1986), considering that the bulk salinity changes very little between the core measurements at the depths of the probes.

It is clear from the graph that the data points from Barrow, the ice tank experiment, and from the probe at 1.45 m depth interval at McMurdo all follow a linear relation between ε' and V_b/V. The reason why the data from the probe at depth 1.25 m in the McMurdo experiment deviates from this line, and is hence excluded, is covered in more detail below.

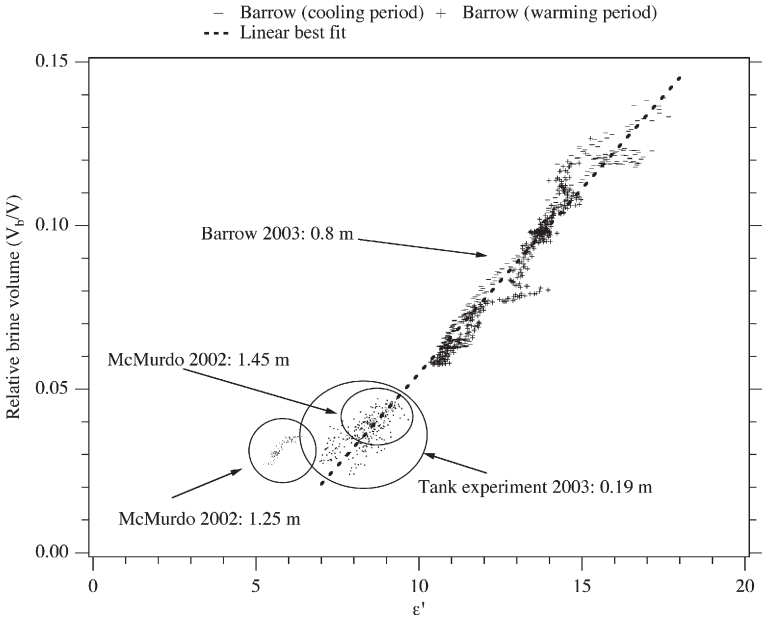

Fig. 8. The relative brine volume V_b/V as a function of the real part of the complex permittivity for all the probes. Data for temperatures above −2 °C are excluded from the calculations. The straight line is a linear best fit to all the data, excluding the probe from McMurdo Sound deployed at depth of 1.25 m.

From Fig. 8 we can develop a linear regression formula that describes the relation between V_b/V and ε':

$$\frac{V_b}{V} = a + b\varepsilon' \tag{5}$$

where a is −0.0582; b is 0.0113; with R^2 as 0.9748.

Eq. (5) can be fitted to an inversion of Eq. (4) to obtain an expression that links the bulk salinity directly with ε', see Eq. (6):

$$S = \frac{1}{\rho} * \frac{(a + b\varepsilon')F_1(T)}{1 + (a + b\varepsilon')*F_2(T)} \tag{6}$$

(for explanation of terms, see Eq. (4)).

Comparing with previous experimental results (Morey et al., 1984; Arcone et al., 1986), this relation should be valid for relative brine volumes at least up to 100‰, with error limits of less than 25% above the percolation threshold. We can suspect that above relative brine volumes of 100‰ the morphology of the brine inclusions have changed so much that the simple assumptions of discrete brine inclusions no longer hold.

We know from thin sections that the Hydraprobes were deployed in columnar ice in Barrow and in the ice tank. If there is a current present, the *c*-axis of the columnar ice crystals will align parallel to it (Weeks and Gow, 1978). This was observed at Barrow with the current parallel to the shore (Cole and Shapiro, 1998), and the probe tines parallel to the *c*-axis of the columnar ice. In the absence of a current in the ice-tank experiment no preferred *c*-axis alignment of the columnar ice crystals was observed. Both Kovacs and Morey (1979) and Morey et al. (1984) showed that if the electrical field is parallel to the preferred *c*-axis alignment of the columnar ice crystals, it will result in a decrease in ε'.

The expected ice-growth at depth in McMurdo is aggregation of so-called platelet ice at the bottom of the ice sheet (Jeffries et al., 1993; Gow et al., 1998; Jones and Hill, 2001; Smith et al., 2001). A vertical thin section from 1.1 to 1.2 m depth at the study site in McMurdo Sound suggests that at this depth interval ice crystals are starting to deviate from the typical columnar structure, with tilted platelets and finer grained ice. Lacking data for the depth interval of 1.2–1.3 meters depth we can assume that the ice has a less well organized structure at this depth, with further platelet accumulations. This, along with higher connectivity between pores, and a reduced degree of anisotropy for such ice, explains much of the observed deviation from the regression curve in Fig. 8, and the lower values of bounds of the apparent aspect ratio observed in Fig. 7A (Golden, personal communication, 2005).

The unexpectedly large values of the bounds of the apparent aspect ratio of the deeper probe could be explained by the presence of the observed milky layer in the core at that depth. Jeffries et al. (1993) and Gow

et al. (1998) did report observing layers of columnar ice interspaced with layers of platelet ice in McMurdo Sound. This could explain the differences in apparent aspect ratio observed by the two probes in the McMurdo experiment.

3.2.3. Salinity change in the landfast sea ice at Barrow, Alaska, 2003

We will now investigate how useful the Hydraprobes are in measuring the salinity changes in sea ice. We chose the data from the Barrow experiment for this, since it is the most complete time series of temperature and dielectric permittivity that we have collected, and because we have good sets of supplementary data to compare the results.

Time series of the relative brine volume and bulk salinity (Fig. 9A and B) of the ice at Barrow have been arrived at by using Eqs. (4) and (6), in conjunction with the data provided by the Hydraprobe. Fig. 9C, showing the daily change in salinity as derived from the salinity data in Fig. 9B, indicates several events during which the bulk salinity of the ice surrounding the Hydraprobe changes rapidly. Fig. 9D shows the temperatures recorded by the Hydraprobe and by the thermistor in the adjacent string deployed at about the same depth as the Hydraprobe. The temperature records are similar but not identical, this is partly due to the fact that the Hydraprobe records the temperature inside the probe casing, while the independent thermistor measures the temperature of the ice itself. Also, the two instruments measure the temperatures at two different locations in the ice. Niedrauer and Martin (1979) showed that the isotherms in sea ice are not horizontal, but vary with the thickness of the ice. The thickness of the ice can vary even over short distances (personal observation by the authors at Barrow, 2003).

Using the independent data provided on the temperature evolution of the ice cover by the thermistor string deployed in conjunction with the Hydraprobe array, we will discuss the salinity evolution and potential brine movement in more detail below.

The thermal evolution of the ice cover is apparent from the contour diagram of daily ice temperatures at depth levels spaced 0.1 m apart (Fig. 10A). Three distinct temperature regimes can be discerned in the ice: (1) rapidly growing ice with a drop in ice temperatures, prior to about day 80 (March 21); (2) a cold stable period, between days 80 and 118 (March 21–April 28), with ice temperatures at the probe's depth level below −5 °C; and (3) early spring warming after day 118 (April 28) to the end of observations in early June, with temperatures between −5 and −2 °C at the probe's depth level.

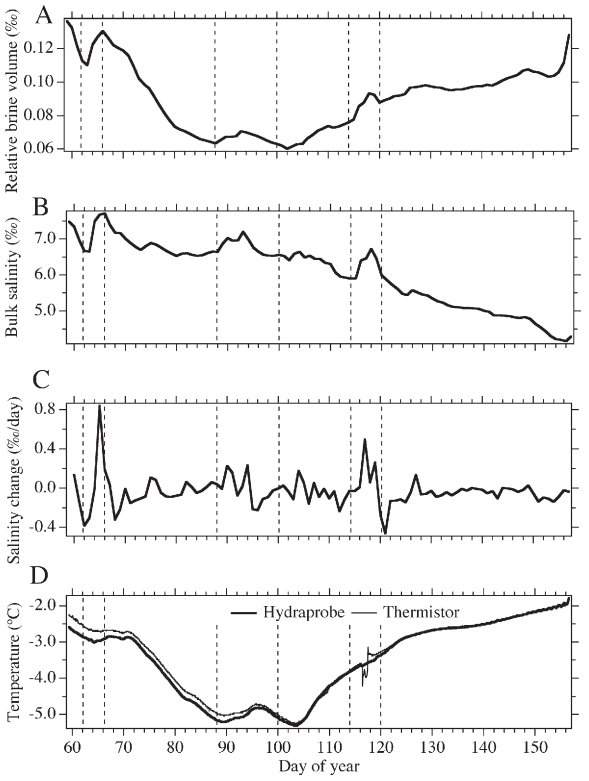

Fig. 9. Relative brine volume (A), bulk salinity (B), and daily change in bulk salinity (C) as derived from dielectric probe data at 0.8 m depth in the landfast ice of the Chukchi Sea near Barrow, Alaska, and temperature (D) as measured by the Hydraprobe and by a thermistor at 0.8 m depth from the adjacent string. Note the large sudden variations in bulk salinity around March 6 (day 65) and April 26 (day 116). Early in the time series, the relative brine volumes are well above 100‰, so the error for these points is most likely significantly larger than 15%. In (D) the similar but slightly different temperature measurements by the two instruments can also be seen. Note especially the very slight temperature change in the Hydraprobe record at day 65, which is not registered by the thermistor, and the strong signal from the thermistor around day 116, which only shows as a slight temperature drop in the Hydraprobe record.

However, it is the connectivity between the brine inclusions that controls the rate of gravity drainage, which is the main desalination mechanism in cold sea ice (Cox and Weeks, 1975). Based on measured salinity profiles, we have estimated the desalination rate from which salinity profiles could be reconstructed at different time points. From these data, in turn, time series of brine volume evolution were derived (Fig. 10B).

In Fig. 10C, one can discern three episodes of apparent brine movement that are above the error limit: around day 65 (March 6), around days 90–95 (March 31–April 5), and around days 115–121 (April 25–May 1).

The third episode takes place in the warming ice temperature regime. In Fig. 9A–C, we see rapid increases

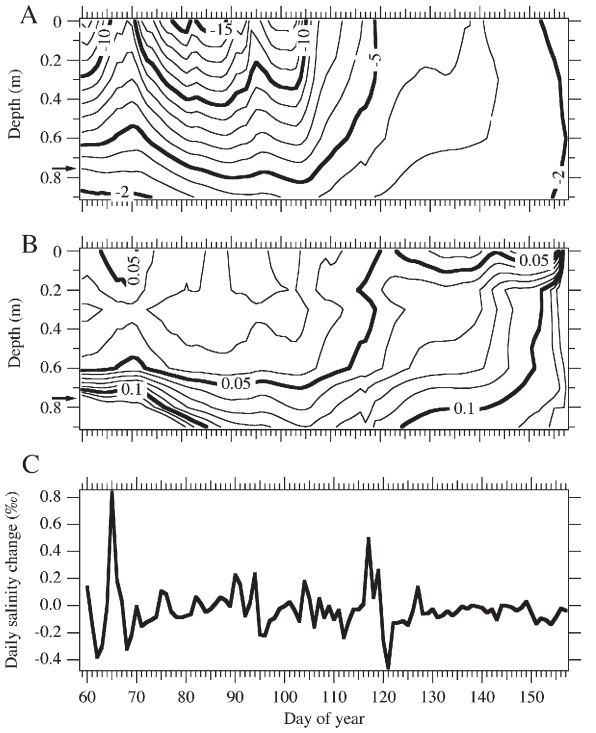

Fig. 10. Contour diagrams of ice temperature in °C (A); relative brine volume in parts per thousand (‰) (B); and daily change in bulk salinity (C) in the landfast ice in the Chukchi Sea outside Barrow, Alaska, 2003. (C) is the same as Fig. 9C, but is included here for ease of comparison. These were calculated using the data provided by the thermistor string and bulk salinity values, obtained from cores retrieved at various times throughout the experiment. The arrow indicates the approximate depth of the Hydraprobe.

in both relative brine volume and bulk salinity, followed by similar decreases. The temperature recorded by the independent thermistor shows a similar decrease followed by an increase (this temperature variation is barely recorded by the thermistor in the Hydraprobe, since it is not sensitive enough). Hudier et al. (1995) recorded a similar thermal event in sea ice, attributing the temperature change to cold dense brine flushing down through porous ice, and then being replaced by seawater from below the lower boundary of the ice. Neither the downward flushing brine nor the seawater that replaces it is in thermal or haline equilibrium with the surrounding ice. Therefore, the ice will first cool as the oversaturated brine dissolves the ice and then warm as latent heat is released by the freezing of the seawater (Worster and Wettlaufer, 1997). Both the brine and seawater will increase the salinity of the already desalinated ice. This effect appears to be temporary, however. We do see from the cores (Fig. 4) that despite desalination of the upper surface of the ice, the bulk salinity of the interior changes very little. The substantial drop in surface salinities does not occur until meltwater flushing starts in late May (Eicken et al., 2002).

It is apparent that this event is not as overturning in a single brine channel, since it is recorded not only by the Hydraprobe and the adjacent thermistor string, but also by the thermistor string deployed 50 m distant (Pringle et al., submitted for publication). This event also coincides with the period when the ice above the probe becomes permeable to brine movement (Golden et al., 1998) as shown in Fig. 10B.

The first of the episodes, around day 65 (March 6), takes place during a period of rapidly growing ice while the probe is still embedded in very porous ice close to the ice–ocean interface. This event is only recorded by the Hydraprobe, not by the independent thermistor (Fig. 9D). This, and the relatively low relative brine volume of the ice above the probe, would lead us to suspect that it is a convective plume of seawater penetrating up into the ice from beneath the ice–ocean interface. Such plumes were observed by Niedrauer and Martin (1979) in laboratory experiments of simulated sea ice.

The second episode takes place between days 90 and 95 (March 31–April 5), during a period of stable, low ice temperatures, when the overall salinity of the ice is fairly stable as well (Fig. 9A). From Fig. 3A and B, it is apparent that this increase in ε' coincides with an increase in temperature. This correlation suggests that the salinity excursion is merely an artifact, resulting from the assumption of a constant desalination rate, which can lead to artificial changes in the derived salinity during periods of stable ice salinity. In contrast, during the second half of the time series, the reduction in bulk ice salinity appears to be captured well, despite increasing temperatures.

3.2.4. Sources of error

There are two sources of error in the experiment: errors stemming from the uncertainties in the measurements of the bulk salinity, and instrument errors. The error limits for the Hydraprobe are given in Table 1. The probe measures average temperature and ε' over its entire volume. However, using the measured values of air temperature and ice thickness, we arrived at an average temperature gradient in the ice of less than 0.2 K/cm for all the experiments. Then, by using the estimated average bulk salinities from the ice cores, we calculated that the contribution to the error in relative brine volume from the instrumental uncertainty is less than 5%.

This indicates that the main source of error for this experiment is the uncertainty in the original bulk salinity

measurements that form the basis of the regression developed in Fig. 8. First, the bulk salinity measurements are averaged over a volume of ice larger than and not directly adjacent to the volume sampled by the probes. Field studies (Bennington, 1967; Tucker et al., 1984) indicate that horizontal variations can be significant, up to 3‰ over distances of 0.25 m. However, parallel cores taken in the homogeneous fast ice at Barrow typically vary by much less than 1‰ at any given depth level. This justifies an estimated error of 0.5‰ in the salinity measurement (Tucker et al., 1984). Secondly, we assume a constant desalination rate between subsequent cores. Our own results and earlier studies by Notz et al. (2005) in growing ice indicate that the brine movements are not continuous, but rather episodical. Studies by Eide and Martin (1975) and Freitag and Eicken (2003) indicate that the main brine movement in sea ice after initial growth takes place within secondary brine inclusion features, for instance, when the initial pores link up to form tubes and channels. For a further investigation of these convective overturnings in sea ice, we refer to Eicken et al. (in preparation).

Thus, there is an error associated with the salinity measurements that enter into Eq. (4). Based on salinity data from ice cores, it appears that the salinities in the Barrow experiment might be overestimated by as much as 20% for the period after initial embedding of the probe in the interior of the ice, and before April 8. There is a similar maximum overestimation of 20% of the bulk salinity in the tank experiment in the period leading up to April 15.

Fig. 7 indicates that the apparent aspect ratios seen by the probes stay constant for temperatures throughout much of the studied temperature interval. We can therefore assume that the brine inclusion morphology does not change significantly within the temperature and complex dielectric permittivity intervals this study focuses on; this assumption is in agreement with the studies by Eicken et al. (2000) and Light et al. (2003). However, further work is needed to validate this assumption and investigate the impact of potential changes in pore morphology on dielectric permittivity measurements.

To calculate the error in the estimate of the bulk salinity, we will have to use the standard formula for error propagation twice: once for Eq. (4) with the error in temperature and the error in the bulk salinity measurement, and then for Eq. (6) with the resulting error in brine volume and the error in temperature. The resulting error in bulk salinity, as measured by the Hydraprobe under the conditions outlined above, is below 15% below the percolation threshold, increasing to 25% as the ice gets close to the melting/freezing temperature.

4. Conclusions

We have presented in this paper results from three separate experiments, in which we have deployed commercially available capacitance probes in natural, undeformed first-year sea ice in the field, and under experimental conditions. We have shown that, within the limitations stated for these experiments, it is possible to measure both the absolute values of the bulk salinity and changes in bulk salinity with large temporal and spatial resolutions, and within a reasonable error limit. This is particularly interesting during periods when rapid desalination of the ice is known to occur, e.g., just after initial freezing and during ice melt, even though, at present, the error limit of our measurements during these periods can be large.

We have concentrated on the real part of the dielectric permittivity ε' in this study. While ε' mainly depends on the relative brine volume and temperature of the ice, the distribution, size, morphology and orientation of the brine inclusions also affect it. These factors increase the overall measurement error, ideally requiring independent data on ice microstructure. At the same time, however, this allows for indirect assessments of changes in microstructure during warming or cooling of the ice, in particular with a set of probes frozen in with different tine/field orientations. The probes also measure the imaginary part of the complex dielectric permittivity, which is more sensitive to the morphology of the brine inclusions. This suggests that with additional information on bulk salinity and ice microstructure from cores (Eicken et al., 2000; Light et al., 2003), the error limits of the bulk salinity measurements can be significantly reduced. At the same time, this offers the possibility to monitor brine pocket evolution using the same techniques described in this paper.

Our results compare well with theory as expressed in the model developed by Tinga et al. (1973). This could be partly due to the brine being mostly concentrated in brine inclusions with large aspect ratios (Light et al., 2003), which provide a large relative contribution to the real value of the complex dielectric permittivity (Addison, 1970). The circular geometry of the probes also makes the absolute orientation of the brine inclusions unimportant in these experiments because of the microstructure of the ice investigated. However, more sophisticated electromagnetic property models may help improve significantly the salinity and brine volume estimates from inversion of permittivity data (Golden, personal communication,

2005), especially for ice which is above the percolation threshold, where more complex brine inclusion morphology is expected, or in frazil or platelet ice, which exhibits a smaller degree of anisotropy than the columnar ice investigated here. This would enable the probes to be used at high temperatures when flushing events take place, and when increases in porosity make the ice more laterally permeable (Cottier et al., 1999; Freitag and Eicken, 2003). Covering the tines with tubing will reduce the probe's sensitivity to contiguous brine concentrations, which would also increase the usefulness of the probe in highly porous ice (Yoshikawa et al., 2004).

The method employed by Notz et al. (2005) in deriving ice salinity from indirect measurements is more sensitive, has better spatial resolution, and works well in the skeletal layer in the ice. However, it only provides the relative concentrations of solid and brine fraction, but does not provide information on the morphology of the brine inclusions. The method described in this paper can be used to model the morphology of the brine inclusions because of the geometry of the Hydraprobe, as described above. Furthermore, our method utilizes relatively cheap, robust, and commercially available probes, which might make it preferable to incorporate them into larger scale studies, such as in the deployment of drifting buoy packages. A further improvement of the capacitance method would include measurements of the capacitance between sensors deployed in parallel vertical boreholes or narrow slits in the ice. Such deployment would be particularly advantageous if it could be achieved without disturbing the ice and without the need for the ice matrix to freeze around the sensors.

Acknowledgements

The research in this paper has been supported by grant NSF-OPP 0126007 from the National Science Foundation. Our thanks go to the 2001–2002 staff at the New Zealand Scott Base, Antarctica, and the staff at the Barrow Arctic Science Consortium for invaluable help with field work and instrument maintenance. We thank Martin Iturri at Stevens Water Monitoring Systems and Dr. Jeffrey Campbell for technical assistance with the Hydraprobe. Thanks also go to Dr. Daniel Pringle for help with the manuscript and to Michael Tapp and Patrick Cotter for help with laboratory work.

References

Addison, J.R., 1970. Electrical relaxation in saline ice. Journal of Applied Physics 41 (1), 54–63.

Arcone, S.A., Gow, A.J., McGrew, S., 1986. Structure and dielectric properties at 4.8 and 9.6 GHz of saline ice. Journal of Geophysical Research 91 (C12), 14281–14303.

Assur, A., 1960. Compostition of sea ice and its tensile strength. CRREL Report, vol. 44. U.S. Army Cold Regions Research and Engineering Laboratory, Hanover, NH.

Bennington, K.O., 1967. Desalination features in natural sea ice. Journal of Glaciology 6 (48), 845–857.

Bitz, C.M., Lipscomb, W.H., 1999. An energy-conserving thermodynamic model of sea ice. Journal of Geophysical Research 104 (C7), 15669–15677.

Campbell, J.E., 1988. Dielectric properties of moist soils at rf and microwave frequencies. Ph.D. Thesis, Dartmouh College, Hanover, NH.

Campbell, J.E., 1990. Dielectric properties and influence of conductivity in soils at one to fifty megahertz. Soil Science of America Journal 54 (2), 332–341.

Chelidze, T.L., Gueguen, Y., 1999. Electrical spectroscopy of porous rocks: a review, I. Theoretical models. Geophysical Journal International 137 (1), 1–15.

Chelidze, T.L., Gueguen, Y., Ruffet, C., 1999. Electrical spectroscopy of porous rocks: a review. II. Experimental results and interpretation. Geophysical Journal International 137 (1), 16–34.

Cole, D.M., Shapiro, L.H., 1998. Observations of brine drainage networks and microstructure of first-year sea ice. Journal of Geophysical Research 103 (C10), 21739–21750.

Comiso, J.C., 2003. Large-scale characterisics and variability of the global sea ice cover. In: Thomas, D.N., Dieckmann, G.S. (Eds.), Sea Ice—An Introduction to its Physics, Chemistry, Biology and Geology. Blackwell, Oxford, UK, pp. 112–143.

Cottier, F., Eicken, H., Wadhams, P., 1999. Linkages between salinity and brine channel distribution in young sea ice. Journal of Geophysical Research 104 (C7), 15859–15871.

Cox, G.F.N., Weeks, W.F., 1975. Brine drainage and initial salt entrapment in sodium chloride ice. CRREL Report, vol. 354. U.S. Army Cold Regions Research and Engineering Laboratory, Hanover, NH.

Cox, G.F.N., Weeks, W.F., 1983. Equations for determining the gas and brine volumes in sea-ice samples. Journal of Glaciology 29 (102), 306–316.

Cox, G.F.N., Weeks, W.F., 1986. Changes in the salinity and porosity of sea-ice samples during shipping and storage. Journal of Glaciology 32 (112), 371–375.

Cox, G.F.N., Weeks, W.F., 1988. Numerical simulations of the profile properties of undeformed first-year sea ice during the growth season. Journal of Geophysical Research 93 (C10), 12449–12460.

Debye, P., 1929. Polar Molecules. Dover Publications Inc., New York.

Dieckmann, G.S., Hellmer, H.H., 2003. The importance of sea ice: an overview. In: Thomas, D.N., Dieckmann, G.S. (Eds.), Sea Ice—An Introduction to its Physics, Chemistry, Biology and Geology. Blackwell, Oxford, UK, pp. 1–22.

Eicken, H., 1992. Salinity profiles of Antarctic sea ice: field data and results. Journal of Geophysical Research 97 (C10), 15545–15557.

Eicken, H., 2003. From the microscopic to the macroscopic, to the regional scale: growth, microstructure and properties of sea ice. In: Thomas, D.N., Dieckmann, G.S. (Eds.), Sea Ice—An Introduction to its Physics, Chemistry, Biology and Geology. Blackwell, Oxford, UK, pp. 22–82.

Eicken, H., Bock, C., Wittig, R., Miller, H., Poertner, H.-O., 2000. Magnetic resonance imaging of sea ice pore fluids: methods and thermal evolution of pore microstructure. Cold Regions Science and Technology 31, 207–225.

Eicken, H., Krouse, H.R., Kadko, D., Perovich, D.K., 2002. Tracer studies of pathways and rates of meltwater transport through Arctic summer sea ice. Journal of Geophysical Research 107 (10), 8046, doi:10.1029/2000JC000583.

Eicken, H., Cole, D.M. Backstrom, L.G.E., Pringle, D. Shapiro, L.H., Trodahl, J., in preparation. Permeability–porosity relationships and convective heat transfer in first-year Arctic sea ice. Journal of Geophysical Resesearch.

Eide, L.I., Martin, S., 1975. The formation of brine drainage features in young sea ice. Journal of Glaciology 14 (70), 137–154.

Fabbri, A., Fen-Chong, T., Coussy, O., 2006. Dielecric capacity, liquid water content, and pore structure of thawing–freezing materials. Cold Regions Science and Technology 44 (1), 52–66.

Freitag, J., Eicken, H., 2003. Meltwater circulation and permeability of Arctic summer ice derived from hydrological field experiments. Journal of Glaciology 49 (166), 349–358.

Golden, K.M., Ackley, S.F., 1980. Modeling of anisotropic electromagnetic reflection from sea ice. CRREL Report, vol. 80-23. U. S. Army Cold Regions Research and Engineering Laboratory, Hanover, NH.

Golden, K.M., Ackley, S.F., Lytle, V.I., 1998. The percolation phase transition in sea ice. Science 282, 2238–2241.

Gow, A.J., Ackley, S.F., Govoni, J.W., Weeks, W.F., 1998. Physical and structural properties of land-fast sea ice in McMurdo Sound, Antarctica. In: Jeffries, M.O. (Ed.), Antarctic Sea Ice: Physical Processes, Interactions and Variability. Antarctic Research Series. American Geophysical Union, Washington, DC, pp. 74355–74374.

Hudier, E.J.-J., Ingram, R.G., Shirasawa, K., 1995. Upward flushing of sea water through first year ice. Atmosphere–Ocean 33, 569–580.

Jeffries, M.O., Weeks, W.F., Shaw, R., Morris, K., 1993. Structural characteristics of congelation and platelet ice and their role in the development of Antarctic land-fast sea ice. Journal of Glaciology 39 (132), 223–238.

Jones, S.J., Hill, B.T., 2001. Structure of sea ice in McMurdo Sound, Antarctica. Annals of Glaciology 33, 5–11.

Kovacs, A., Morey, R.M., 1979. Anisotropic properties of sea ice in the 50- to 150-MHz range. Journal of Geophysical Research 84 (C9), 5749–5759.

Leppäranta, M., Manninen, T., 1988. The brine and gas content of sea ice with attention to low salinites and high temperatures. Finnish Institute of Marine Research Internal Report, vol. 88-2. Helsinki, Finland.

Light, B., Maykut, G.A., Grenfell, T.C., 2003. Effects of temperature on the microstructure of first-year Arctic sea ice. Journal of Geophysical Research 108 (C2), 3051, doi:10.1029/2001JC000887.

Maykut, G.A., 1986. The surface heat and mass balance. In: Untersteiner, N. (Ed.), The Geophysics of Sea Ice. Plenum Press, New York, pp. 395–463.

Moore, J.C., Maeno, N., 1993. Dielectric properties of frozen clay and silt soils. Cold Regions Science and Technology 21, 265–273.

Morey, R.M., Kovacs, A., Cox, G.F.N., 1984. Electromagnetic properties of sea ice. CRREL Report, vol. 80-20. U. S. Army Cold Regions Research and Engineering Laboratory, Hanover, NH.

Nakawo, M., Sinha, N.K., 1981. Growth rate and salinity profile of first-year sea ice in the high Arctic. Journal of Glaciology 27 (96), 315–330.

Niedrauer, T.M., Martin, S., 1979. An experimental study of brine drainage and convection in young sea ice. Journal of Geophysical Research 84 (C3), 1176–1186.

Notz, D., Wettlaufer, J.S., Worster, M.G., 2005. A non-destructive method for measuring the salinity and solid fraction of growing sea ice in situ. Journal of Glaciology 51 (172), 159–166.

Perovich, D.K., Gow, A.J., 1996. A quantitative description of sea ice inclusions. Journal of Geophysical Research 101 (C8), 18327–18343.

Pounder, E.R., 1965. The Physics of Ice. Pergamon Press, Oxford, UK.

Pringle, D.J., Eicken, H., Trodahl, H.J. and Backstrom, L., submitted for publication. Thermal conductivity of land-fast Antarctic and Arctic sea ice. Journal of Geophysical Research.

Schwarzacher, W., 1959. Pack ice studies in the Arctic Ocean. Journal of Geophysical Research 64 (12), 2357–2367.

Smith, I.J., Langhorne, P.J., Haskell, T.G., Trodahl, H.J., Frew, R., Vennel, M.R., 2001. Platelet ice and the land-fast sea ice of McMurdo Sound, Antarctica. Annals of Glaciology 33, 21–27.

Stevens Water Monitoring Systems, 1994. Hydra soil moisture probe user's manual version 1.2 with floppy disk. Stevens Water Monitoring Systems, Beaverton, OR.

Stogryn, A., 1987. An analysis of the tensor dielectric constant of sea ice at microwave frequencies. IEEE Transactions on Geoscience and Remote Sensing GE-25 (2), 147–158.

Tinga, W.R., Voss, W.A.G., Blossey, D.F., 1973. Generalized approach to multiphase dielectric mixture theory. Journal of Applied Physics 44 (9), 3897–3902.

Tucker, W.B., Gow, A.J., Richter, J.A., 1984. On small-scale horizontal variations of salinity in first-year sea ice. Journal of Geophysical Research 89 (C4), 6505–6514.

Untersteiner, N., 1968. Natural desalination and equilibrium salinity profile for perennial sea ice. Journal of Geophysical Research 73 (4), 1251–1257.

Vant, M.R., 1976. A combined empirical and theoretical study of the dielectric properties of sea ice over the frequency range. Ph.D. Thesis, Carleton University, Ottawa, Canada.

Vant, M.R., Ramseier, R.O., Makios, V., 1978. The complex-dielectric constant at frequencies in the range 0.1–40 GHz. Journal of Applied Physics 49 (3), 4712–4717.

Weeks, W.F., Ackley, S.F., 1986. The growth, structure and properties of sea ice. In: Untersteiner, N. (Ed.), The Geophysics of Sea Ice. Plenum Press, New York, pp. 9–164.

Weeks, W.F., Gow, A.J., 1978. Crystal alignment in the fast ice of Arctic Alaska. Report, vol. 79-22. U. S. Army Cold Regions Research and Engineering Laboratory, Hanover, NH.

Worster, M.G., Wettlaufer, J.S., 1997. Natural convection, solute trapping, and channel formation during solidification of saltwater. Journal of Physical Chemistry B 101 (32), 6132–6136.

Yoshikawa, K., Overduin, P.P., Harden, J.W., 2004. Moisture content measurements of moss (*Sphagnum* spp.) using commercial sensors. Permafrost and Periglacial Processes 15, 309–318.